1

Modeling and Optimization in Manufacturing by Hydroforming and Stamping

Hakim Naceur[1] and Waseem Arif[2]

[1] *Université Polytechnique Hauts-de-France, CNRS, INSA Hauts-de-France, UMR 8201-LAMIH, F-59313 Valenciennes, France*
[2] *University of Gujrat, Mechanical Engineering Department, Gujrat, Pakistan*

1.1 Introduction

Due to the strict environmental policies and shortage of energy, the manufacturing industries are pressurized to cut down the raw material cost and to save energy. This is particularly true in the automotive industry, where manufacturers are obliged to develop advanced techniques to reduce the pollution by reducing the fuel consumption without significant increase in the cost. Among all the manufacturing techniques, the stamping and hydroforming methods hold a top position among the cold sheet metal forming processes due to the versatility of components that can be produced and high production rates [1]. Stamping and hydroforming processes are intensively used in various industrial sectors such as transportation, car body in white (Figure 1.1), household appliances, metal packaging, etc.

The use of fluid pressure has been remarkably increased in sheet metal forming processes since it allows a superior final surface quality of the workpiece than standard deep drawing process [2–4]. In particular, sheet hydroforming process has great potential to manufacture body-in-white parts with consistently extreme level of ultimate tensile strength, reduced weight, geometrical accuracy, and minimum tolerances. It has certain advantages, e.g. more uniform thickness distribution of the final workpiece component, lower tooling cost, and versatility to produce parts with different geometries using the same setup [5].

The worldwide acknowledgment of these two sheet metal forming processes is largely due to the external pressure from the government legislators to develop lightweight products.

Stamping and hydroforming processes will be discussed in this chapter, the aim of which is to present an overview of the most recent research investigations done in

Modeling and Optimization in Manufacturing: Toward Greener Production by Integrating Computer Simulation, First Edition. Edited by Catalin I. Pruncu and Jun Jiang.

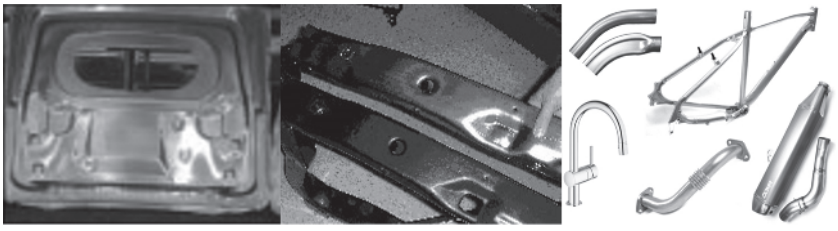

Figure 1.1 Examples of parts obtained by stamping and hydroforming. Source: Hakim Naceur.

the field of numerical simulation and parameters optimization of forming processes. This chapter is split into in two main topics:

- *Numerical simulation of deep drawing and hydroforming processes*: In this section, recent advances in the numerical simulation by finite element method for deep drawing and hydroforming of thin metallic sheets will be covered.
- *Design and optimization of deep drawing and hydroforming parameters*: The aim of this section is to cover recent research works in the field of design and numerical optimization applied to deep drawing and hydroforming processes to improve the quality of the final workpiece by calculating "ideal" process parameters.

1.2 Recent Advances in Stamping and Hydroforming Simulation

Both stamping and hydroforming processes belong to the manufacturing of complex sheet metallic parts from a flat or curved blank of small thickness (Figure 1.2a). The tube hydroforming process starts with a hollow cylindrical metal tube filled with fluid and expanded to a more complex geometry (Figure 1.2b). The material thinning can be reduced by increasing simultaneously the fluid pressure on the inside of the tube while feeding new material and axial feeding [6]. The tube can be obtained in several ways. For instance, by bending and welding of a rectangular plate; later it takes the shape of the mold by the application of internal pressure and bi-axial opposite loads on their ends which do not always have the same magnitude. In the stamping process, the blank is pressed with a certain force against the die, maintained using the blankholder, and shaped by moving the punch using a deep drawing press.

Numerical methods for deep drawing and hydroforming simulation must, as far as possible, take into account different combinations of nonlinear behavior such as the large elastoplastic strains, contact with friction, and large displacement/rotations, which generate a strongly nonlinear system of equations that need to be solved accurately to represent the physical state of the material at different stages of the forming process. Numerical resolution methods, used to solve the forming simulation process, can be classified in two main categories:

1. *Direct methods*: On the basis of the full knowledge of the tool geometry and the blank/tube in its initial state (computer aided design [CAD] geometry, material,

process parameters), experts in the field are able to simulate and predict the intermediate and final configurations of the workpiece by taking into account the stresses and geometric conditions imposed by available tools. These methods are precise but complex and need a high engineering expertise to carry out the solution correctly.

2. *Inverse methods*: On the basis of the knowledge of the desired final CAD geometry of the workpiece and the material parameters of the initial blank, experts in the field are able to predict thickness distribution and the shape of the initial blank or length of tube. Inverse methods are very fast and generally used to study the influence of different process parameters and analyze the feasibility of a workpiece.

Generally there exist two types of algorithms to predict stress and strain evolution by using displacement increments. The first family is based on the "implicit statics," where the Updated Lagrangian formulation is generally used and coupled with a Newton–Raphson method to check the equilibrium at each iteration within the same time step. Some commercial softwares are based on this algorithm, such as ABAQUS Standard, LS-DYNA Implicit, ANSYS, INDEED, MARC, etc. The "implicit statics" algorithm allows obtaining results of high accuracy for using significant computation times, since to ensure convergence a high number of load step is generally needed. This family of algorithms may also exist in an explicit form which is rarely used. The second family is based on "explicit dynamics" taking into account inertia forces in the system of equilibrium equations. The resulting partial differential system of equations can be integrated in time using the Newmark explicit integration scheme. Using this algorithm helps avoid convergence problems and save memory

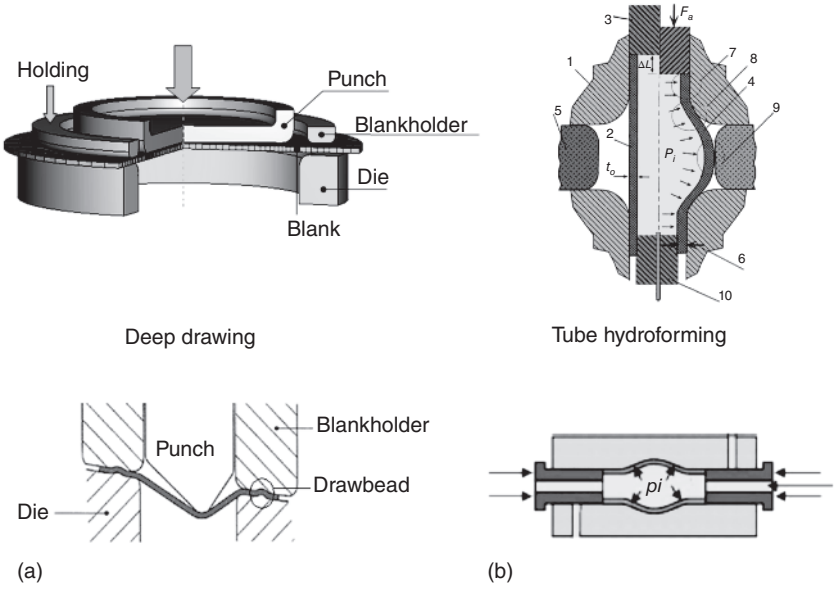

Figure 1.2 Principle of sheet metal forming processes: (a) stamping, (b) hydroforming.

space. Nevertheless, the results are less accurate but the main advantage is the computation time which remains small enough compared to the "implicit statics" algorithm. Numerous commercial softwares based on the "explicit dynamics" algorithm exist, such as LS-DYNA, PAM-STAMP, RADIOSS, ABAQUS Explicit, etc.

The major drawbacks of incremental approaches remain the huge computing time and the need to have a high expertise engineer for the adjustment of their numerous parameters. Hence, it possible to carry out validation of appropriate tooling by performing a full simulation of different complex forming stages of a given part.

While analysis tools based on simplified approaches have been developed mainly for the preliminary design stages of a part, these simplified approaches use a prior knowledge of the final shape of the workpiece, which makes it possible to know the vertical displacement of each point. A comparison with the initial blank or tube allows a good estimation of the elastoplastic strain by retaining certain simplifying assumptions on the material behavior and the actions of tools. Generally they are based on a constitutive law of Hencky type within the framework of total plastic deformation theory. Contact processing is limited to calculating nodal actions on the final workpiece. The advantage of this type of approach lies in their ease of use and speed of execution making them very useful during the early design stage of a new part.

1.2.1 Fast Nonlinear Procedures in Stamping and Hydroforming

The Inverse Method uses the knowledge of the initial thickness and shape of the deformed workpiece while the initial blank/tube configuration as well as the final strain and thickness distributions constitute the solutions of the problem. The analysis is performed assuming that the deformation is independent of the loading path [7]. The Inverse Method has been studied by numerous authors such as Guo et al. [8, 9], Batoz et al. [10], Chung et al. [11, 12], Lee and Huh [13]. Authors, showed that the Inverse Method can predict accurately the formability of a part compared to results obtained using incremental analysis or experiments. In the applications considered by those authors, flat sheet forming problems were analyzed.

From a mesh of the final workpiece, positions of the material points in the initial blank/tube are targeted (Figure 1.3). The first estimate can be the simple orthogonal projection of the nodes in the horizontal plane (or onto the cylindrical surface of the initial tube in the case of hydroforming); then these positions are enhanced using an implicit Newton–Raphson algorithm to satisfy the mechanical equilibrium of the final workpiece. Two main assumptions are generally adopted, i.e. the proportional

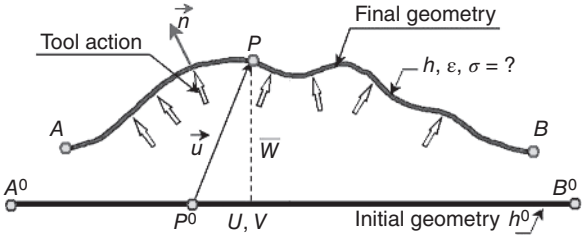

Figure 1.3 General description of the Inverse Method.

loading assumption, which allows the use of Hencky integrated law, the simplified action of tools, which allows these actions to be replaced by nodal forces avoiding the contact problem. Thus, we obtain a method independent of the loading history. The basic version of the Inverse Method proves to be very fast and robust for estimating large deformations of thin metallic sheets obtained by stamping and hydroforming.

Since its development, several research investigations have been done to improve the performances of the Inverse Method – in particular, by the proposal, development, and validation of several variants of the Inverse Method based on the principle of the minimum of the total potential energy leading to a symmetrical tangent matrix, thus making it possible to deal with problems of larger sizes (see reference [14]). Another research work that is related to the robustness of the Inverse Method consists in improving the initial solution of the Newton–Raphson algorithm, using essentially digital geometry processing allowing a very fast convergence for the resolution of the nonlinear problems (see references [15, 16]).

Indeed, in the basic Inverse Method, convergence problems may arise, especially when simulating the forming of parts with vertical walls or substantial depths. Sections 1.2.1.1, 1.2.1.2 and 1.2.1.3 will be summarized three algorithms for generating initial mesh using different unfolding procedures to predict the initial guess to enhance the convergence of the Newton–Raphson algorithm.

1.2.1.1 Geometrical Mapping Algorithm

This technique is particularly suitable for cylindrical of axisymmetric parts. It is inspired from adaptive sampling of implicit surfaces to estimate the initial positions of the material points in the flat blank (or initial tube) from their positions in the final 3D surface. This method is based on the theory of axisymmetric surface and the assumption of volume incompressibility. The method has been generalized to the three-dimensional case, but its application is useful only in the case of parts having a quasi-axisymmetric shape (see Figure 1.4). For more details, the reader can refer to the references [15, 16].

1.2.1.2 Radial Length Development Algorithm

The "geometrical mapping algorithm" allowed good results in the case of workpieces of cylindrical shape with relatively coarse meshes. An algorithm called "radial length development" has been developed. It uses the curvilinear length between a central knot near the gravity center of the workpiece and any knot in the radial direction from the gravity center. The development is done in the radial direction by considering the center of gravity as a fixed point while all surrounding nodes are moved (see Figure 1.5). This algorithm has been tested for the unfolding of different parts of simple to complex shapes. It has shown greater stability than the previous algorithm. The technical details related to the numerical procedure can be found in the references [15, 16].

1.2.1.3 Orthogonal Length Unfolding Algorithm

The previously mentioned two algorithms improved the convergence of the Inverse Method when the workpiece shape is close to an axisymmetric shell. In the case

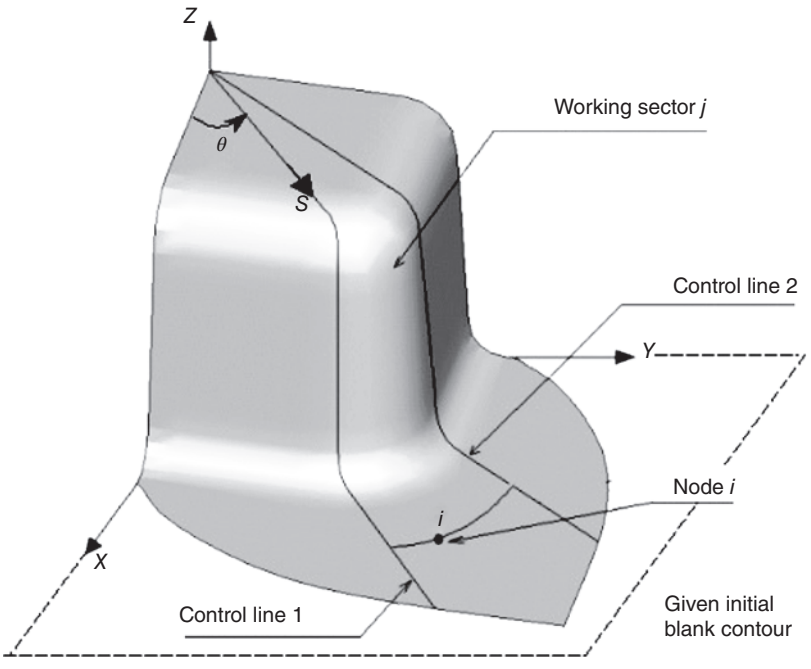

Figure 1.4 Geometrical mapping method.

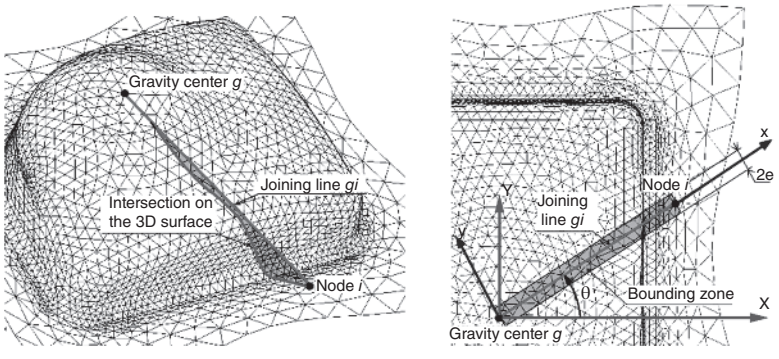

Figure 1.5 Radial length development algorithm.

of long or complex geometric shapes such as those of Figure 1.6, the two previous algorithms diverge and cannot allow unfolding the 3D workpiece mesh to generate a good initial solution.

Figure 1.6 shows that it is wise to perform the length unfolding from a central line in the orthogonal directions instead of the radial length development from a gravity center. A central curve generated from the part profile was used to produce orthogonal projection directions, instead of the radial development from the center of gravity. The orthogonal length unfolding algorithm is based on the following steps:

1. Generation of a central curve for orthogonal development.
2. Balance of the 3D workpiece in order to find the best forming direction and to avoid undercuts.
3. Numerical opening of vertical walls, if balance is not enough.
4. Orthogonal unfolding of the walls based on the central curve.

This method allows one to find a good estimate of the initial blank; therefore, it provides a good initial guess for the Newton–Raphson algorithm and thus enhance convergence of the Inverse Method. Table 1.1 summarizes numerical results using the orthogonal length unfolding algorithm compared to the standard vertical projection. One can notice that in spite of the complexity of the part shown in Figure 1.6, convergence was obtained in only a few iterations unlike vertical projection. For more details, the reader can refer to the references [15, 16].

There are several other research works to improve the performance of the Inverse Method, in particular for:

- Proposal and test of a dynamic relaxation algorithm for the resolution of the nonlinear problem as an alternative to the resolution using the implicit statics with Newton–Raphson algorithm.
- Integration of iterative solver allowing to deal with complex applications with very fine meshes having more than several millions of elements.

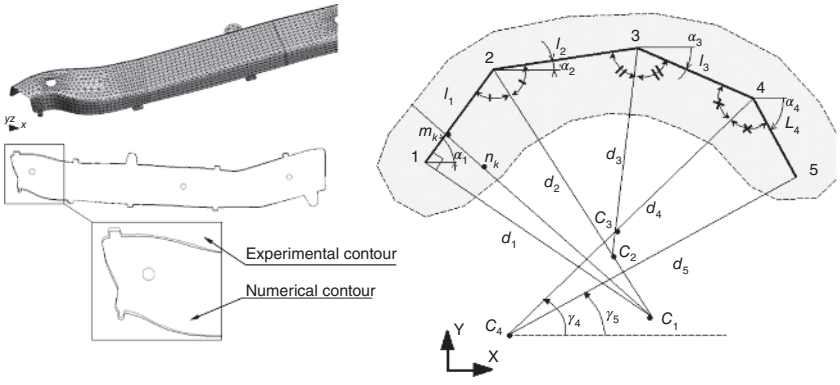

Figure 1.6 Orthogonal length unfolding algorithm.

Table 1.1 Convergence results of the orthogonal length unfolding algorithm.

Iterate	Vertical projection		Orthogonal unfolding	
	Displacement norm	Residual norm	Displacement norm	Residual norm
1	1.0000E+00	1.0000E+00	1.0000E+00	1.0000E+00
2	********	********	5.7340E−01	4.0445E−01
3	********	********	9.0225E−01	9.3546E−02
4	********	********	1.7957E−01	3.0110E−03
5	********	********	2.4524E−03	4.2155E−06

- Realization of a user-friendly graphical interface for improving the pre- and post-processing of the data [17–19].
- Development and validation of a new variant of the Inverse Method based on the principle of the minimum of the total potential energy leading to a symmetrical tangent matrix (see reference [14]).

1.2.2 Multistage Inverse Method for Stamping and Hydroforming

In the initial design phase, it is interesting to use a simplified method to obtain a good estimate of the stress states. The single-step Inverse Method [9, 16, 18] has shown that it can give a fairly good strain estimation at very low computational time, but the estimation of the stress remains poor. This is due to the radial loading assumption for the estimation of stresses (Figure 1.7).

In our research work, a Multistage Inverse Method (MIM) is continuously under development [20–22] to take into account the history of deformations. The main features of this method are:

- Introduction of realistic intermediate configurations for the calculation of the strain increment between two successive configurations. These configurations are determined upstream of the inverse calculation, without conventional treatment of contact.
- Calculation of constraints taking into account the loading history by an implicit integration method.

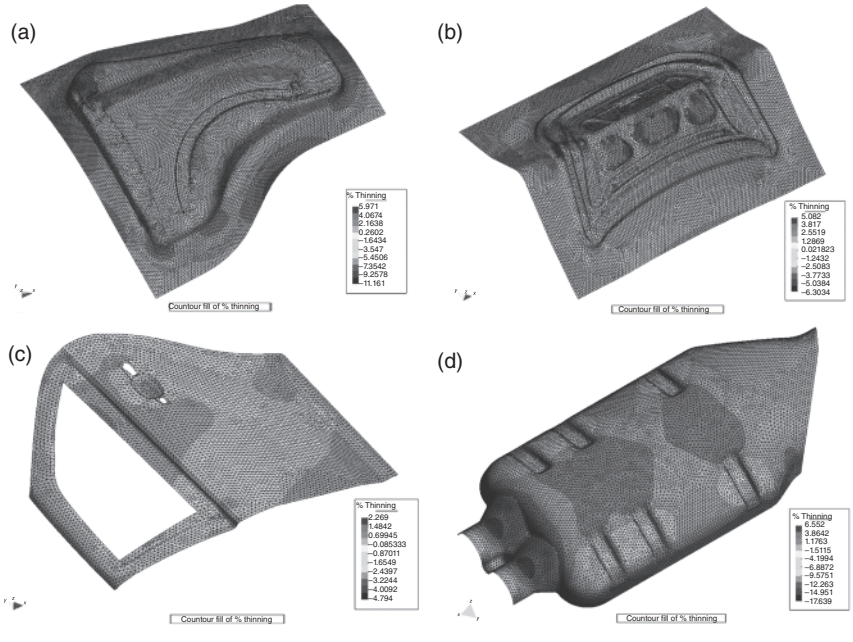

Figure 1.7 Examples of industrial stamped parts produced by the Inverse Method. Source: Based on Batoz et al. [19].

- Mapping results from one step to another by specific procedures which respect the equilibrium conditions.

1.2.2.1 Generation of Intermediate Configurations

Consider a thin metallic sheet located between the die and the punch before the end of its maximal stroke. We assume that the shape of the sheet is tangent to the tools, thus behaving like a stretched membrane. The shape can be determined by minimizing the sheet area. This allows minimizing the length of the metallic sheet profile, taking into account the constraints due to the tool geometry (see Figure 1.8).

Let C_M, C_P, and C_T be the configurations of the die, the punch, and the blank sheet, respectively. The mesh of the die (C_M) is created on the final workpiece of known shape, the mesh of the punch (C_P) is obtained by a vertical translation of C_M, and the mesh of the sheet (C_T) remains unknown to be determined. The nodes of the three meshes have the same radial coordinates r_i and different vertical coordinates (z_{Mi}, z_{Pi}, and z_{Ti}). Taking the vertical coordinates z_{Ti} of the blank sheet as design variables and the profiles of the tools as constraints, an optimization problem can be stated as follows:

$$Min \sum_{i=1}^{n-1} d_i^2 \tag{1.1}$$

with

$$d_i^2 = (r_{i+1} - r_i)^2 + (z_{Ti+1} - z_{Ti})^2 \quad z_{Pi} \leq z_{Ti} \leq z_{Mi} \tag{1.2}$$

where n is the number of knots on the blank profile.

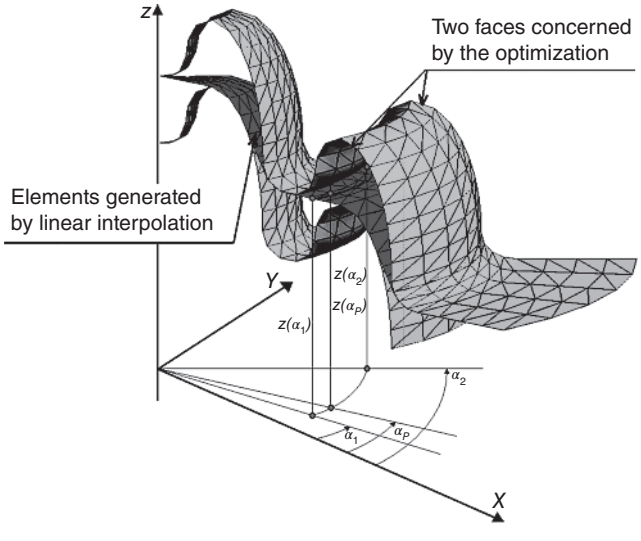

Figure 1.8 Length minimization of the metallic sheet profile.

1.2.2.2 Integration of Stress States

To keep the advantages of the Inverse Method, the total strains are calculated at each iteration between the initial and current configurations; hence the increment of strain can be estimated. The constitutive law is not capable of taking into account the history of loading, and therefore it is replaced by an incremental stress integration approach based on an implicit algorithm (Radial Return algorithm).

To predict the plastically admissible stresses verifying the anisotropic plasticity criterion of Hill48, the latter is expressed according to the plastic multiplier λ and a one-dimensional line search is carried out for the calculation of λ such that the criterion of plasticity is verified.

Let $\{\sigma^0\}$ and $\overline{\varepsilon}_p^0$ be the initial yield stress and the equivalent plastic strain respectively to be known at the beginning of a step: these quantities correspond to the estimated stresses and strains (obtained) from the previous intermediate configuration. $\{\Delta\varepsilon\}$ is the strain increment of the step, with $\{\Delta\varepsilon\} = \{\varepsilon\} - \{\varepsilon^0\}$, $\{\varepsilon^0\}$ predicted from the previous configuration, $\{\varepsilon\}$ target strain of the current configuration. These strains are calculated using the standard Inverse Method. $0 < \alpha < 1$ is the parameter of the semi-implicit algorithm. The total stress at iteration i $\{\sigma^t(\Delta\lambda)\}$ can then be estimated using

$$\{\sigma^i\} = ([I] + \alpha\Delta\lambda[H_e][P])^{-1}(([I] - (1-\alpha)\Delta\lambda[H_e][P])\{\sigma^0\} + [H_e]\{\Delta\varepsilon\}) \quad (1.3)$$

The equivalent plastic strain can also be expressed as

$$\overline{\varepsilon}_p^i = \overline{\varepsilon}_p^0 + \Delta\lambda(\{\sigma^\alpha\}^T[P]\{\sigma^\alpha\})^{1/2} \quad (1.4)$$

Thus, the plasticity criterion becomes a function of $\Delta\lambda$. The application of Newton–Raphson algorithm allows predicting $\Delta\lambda$ by verifying the plasticity criterion. The flowchart for the algorithm is depicted in Figure 1.9.

At convergence, $\Delta\lambda$, $\{\sigma^i\}$, and $\overline{\varepsilon}_p^i$ are obtained. Note that the integration of plasticity takes place on a step (cumulative strains since the beginning of a step) and not on an iteration in order to avoid the problem of wrong elastic unloading caused by equilibrium iterations.

The plastic integration algorithm allows taking into account the loading history, in particular the bending/unbending effects of the metallic sheet, during its sliding between the tools. Taking these effects into account is essential for the estimation of an accurate stress state and therefore a good springback prediction.

1.2.2.3 Procedure for Mapping Fields between Two Configurations

In Section 1.2.2.2, a geometric procedure generate intermediate forming configurations, has been presented for different prescribed punch positions. These CAE configurations are completely independent, which means that a node i belonging to two intermediate CAE configurations does not represent the same material point. It is therefore necessary to perform a mapping of fields to localize material points from the initial configuration to the final workpiece. From each of the CAE configurations, the Inverse Method allows the prediction of initial positions of nodes in the initial blank or initial tube. The initial position represents a good reference for

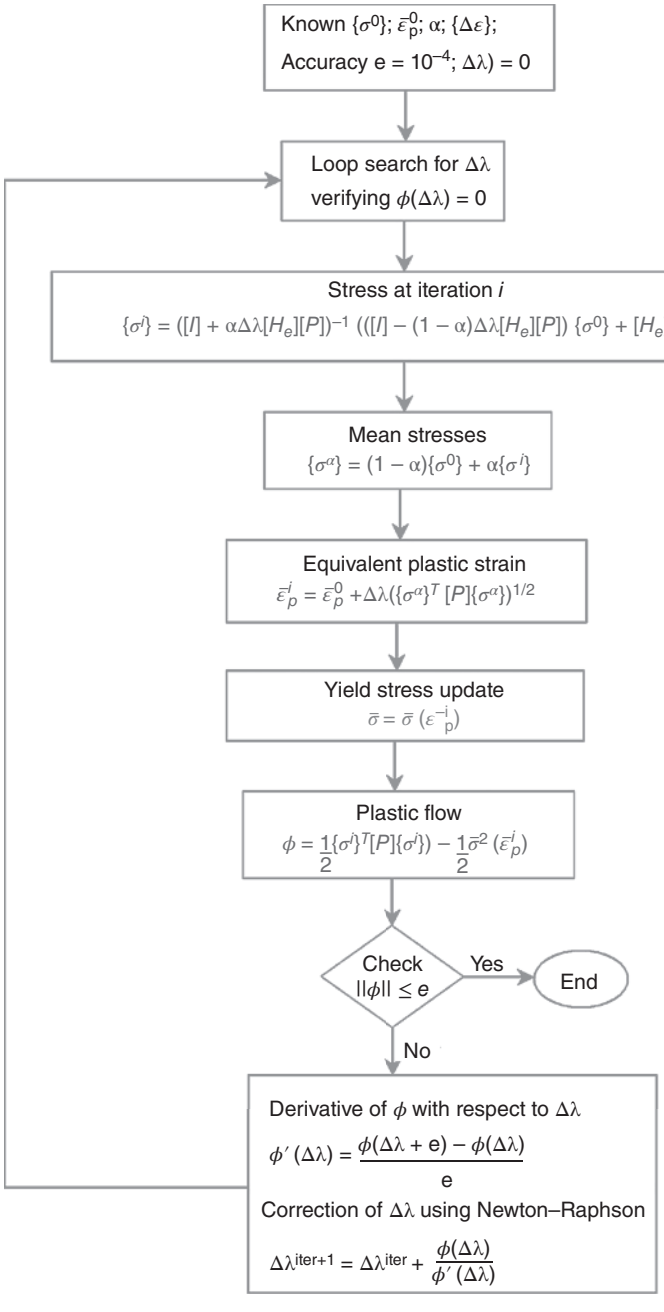

Figure 1.9 Radial mapping algorithm for stress calculation in the multistage Inverse Method.

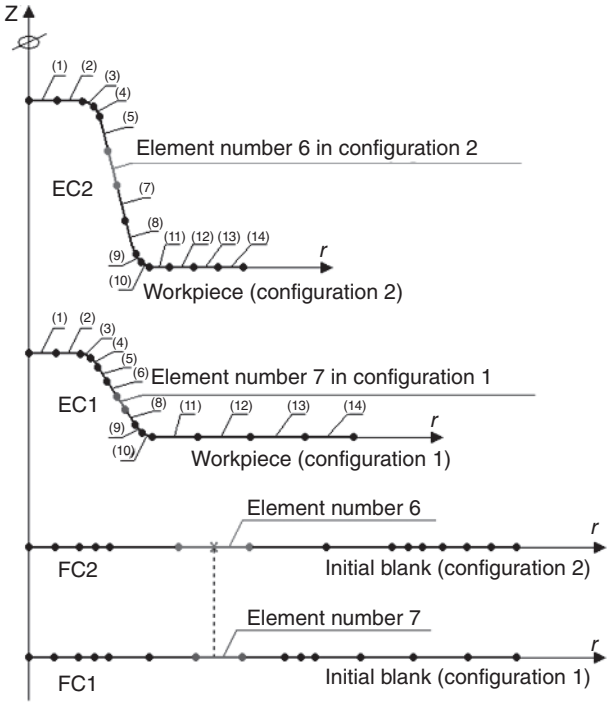

Figure 1.10 Mapping of fields between two configurations.

mapping the results of plastic strains and stresses and finally identifying the material flow history.

Let us consider a two-step inverse simulation (Figure 1.10). At the first step, the mesh of the workpiece *EC*1 allows obtaining the mesh of the initial flat blank *FC*1 together with the strain and stress states in *EC*1. In the second step, the mesh *EC*2 allows obtaining the initial flat blank *FC*2. If one needs to predict the deformation history of element 6 (in *EC*2) for example, at first one needs to estimate its initial position in *FC*2. Let us suppose that its position corresponds to element 7 in *FC*1. Thus, one can use the information of element 7 at the first stage (*EC*1) and then calculate the strains and stresses of element 6 at the second stage. Note that a coarse discretization can introduce errors in this transformation of information.

1.2.2.4 Application to the Demeri Cylindrical Cup

This example was proposed and studied experimentally and numerically by M.Y. Demeri from the laboratory of the Ford company [17, 23, 24]. It consists of a first stamping operation to obtain a cylindrical cup followed by a second cutting operation to obtain a circular ring and a final radial splitting operation to open up the ring due to residual stresses as shown in Figure 1.27. In the present application, only the first stamping operation will be discussed.

Anisotropy coefficients $r_0 = r_{45} = r_{90} = 0.64$
Hardening law $\bar{\sigma} = 488.01\ \varepsilon^{0.232}$ MPa
Initial thickness $h^0 = 1.6$ mm
Punch stroke $Z = 56$ mm
Young's modulus $E = 69\,000$ MPa
Poisson's ratio $V = 0.33$
Density $p = 2.65\ 10^{-6}$ kg/mm^3
Holding force $F = 30$ KN
Punch velocity $V = 5$ m/s
Yield stresses $Re_0 = Re_{45} = Re_{90} = 109.3$ MPa
Friction coefficient $\mu = 0.12$

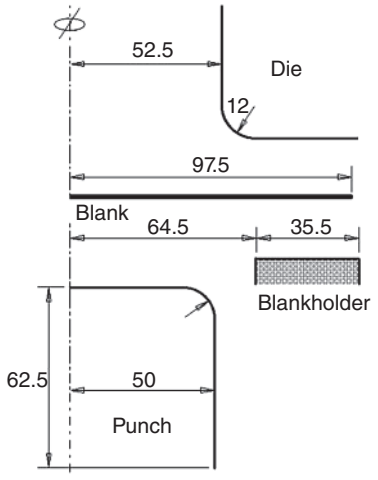

Figure 1.11 Geometrical and mechanical description of the Demeri cylindrical cup.

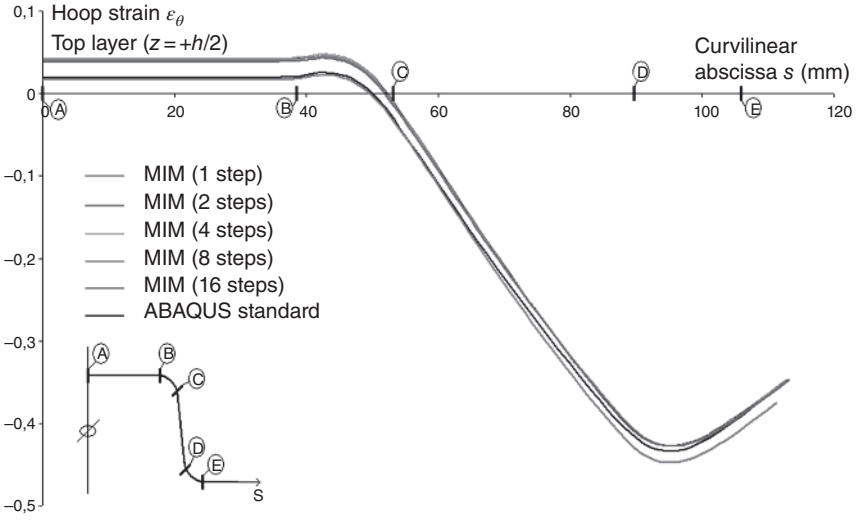

Figure 1.12 Distribution of hoop strain on the upper layer.

The geometrical and mechanical characteristics are given in Figure 1.11. The sheet was meshed using 60 two-node axisymmetric shell elements.

Regarding the strain distributions shown in Figure 1.12, one can notice that the results of the MIM are quite close to those obtained using ABAQUS Standard. In addition, one can remark that by increasing the number of steps from one to sixteen, the obtained solution remains stable. The situation is completely different for stress distribution depicted in Figure 1.13. Indeed, the MIM using a single step shows a bad prediction of stresses in some regions of the sheet, which are very far compared to the

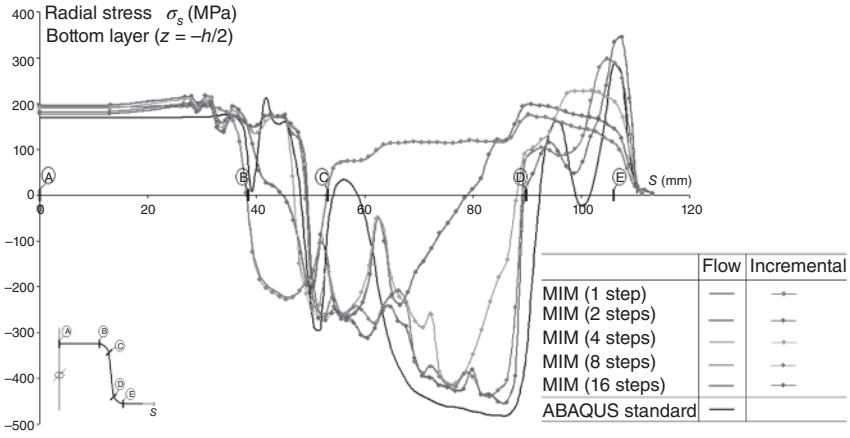

Figure 1.13 Distribution of radial stresses on the lower layer.

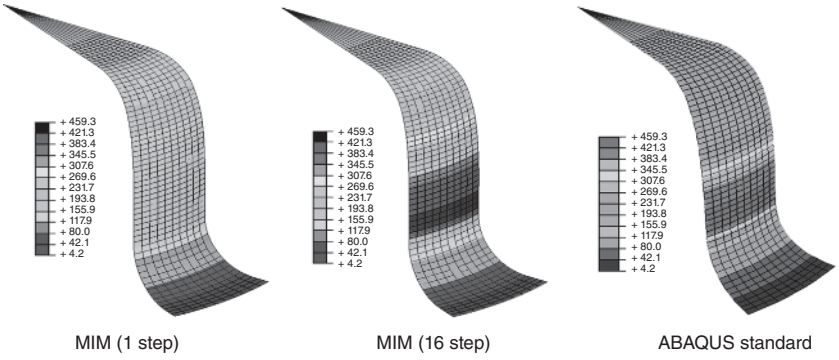

Figure 1.14 Contour plots of the radial stress on the upper layer.

reference solution of ABAQUS standard. The region where this difference manifests is located between the punch and die radii (the free walls).

Since the Demeri cylindrical cup is very deep compared to the radius which represents a zone of 40 mm height. Each element of this region has undergone a bending after crossing the die radius the first time, then an unbending after it becomes flat again. Therefore, elements in this zone have accumulated high plastic strains which directly affects the stress state.

The numerical results of MIM depicted in Figure 1.14, show a good convergence compared to the reference solution of ABAQUS Standard software. Indeed, one can remark that by using only four steps, the MIM converges to the reference solution. Therefore, it constitutes an alternative way for sheet metal forming simulation since it allows a very fast computational time compared to ABAQUS Standard. Field mapping operations are mandatory between two successive configurations and the generation of a good initial solution presented previously guarantees a systematic convergence.

1.2.3 Improved Inverse Method for Stamping and Hydroforming

1.2.3.1 Basic Idea

According to previous investigations [20, 21], it has been shown that the Inverse Method allows a good prediction of strains but the stress distribution remains poor, especially in the regions located between the punch and the die. This is mainly due to the absence of deformation history for material points which undergo bending and then unbending loading when crossing the die entrance radius. In Sections 1.2.3.2–1.2.3.5, new considerations have been included to the Inverse Method allowing an accurate version called, in this chapter, "Improved Inverse Method," which takes into account in an original manner the bending and unbending effects while keeping a single calculation time step.

1.2.3.2 Deformation Path Prediction

As stated previously, the basic Inverse Method does not allow a good stress prediction especially in the contact-free workpiece zone located between the punch and the die. This is due to the fact that in the Inverse Method only initial and final configurations are compared to predict the strains and stresses in a given material point.

For elements that have crossed bending and unbending zones (die entrance radius), stresses obtained by the Inverse Method have been shown to be very far from the reference solution. In Section 1.2.3.3 an original and fast procedure to determine approximately the deformation path for a given finite element from its starting position in the initial blank and its final state in the workpiece is discussed.

Let us consider the two configurations C and C_0 shown in Figure 1.15. A point p_0 belonging to an element in the initial blank is chosen. The point p_0 after stamping is found in position p_1 (see Figure 1.15). In order to know if the tracked point p_0 has crossed the matrix entrance line, one needs to proceed as follows: At first, the displacement vector $p_0'p_1$ is projected on the final surface of the stamped workpiece, which allows determining the curve which belongs to the surface of the workpiece.

Then, in order to determine whether the point p_0 has crossed the die entrance line, a simple intersection between the curve p_0p_1 and the die entrance line cc' is projected. If the intersection generates a point, it means that the point has crossed the die entrance line, otherwise not.

Once this first stage is done, the maximum curvature is assigned to the elements which are located in the potential zone. For instance, in the case of the stamping test of the "U" sheet, this maximum curvature is simple and reads $1/r_m$, where r_m is the main curvature which represents the die entrance radius.

1.2.3.3 Consideration of Bending Moments

Once the curvatures are estimated from the mesh and based on the formulas in Section 1.2.3.2, the second step would be to estimate the bending and unbending moments at the die entrance radii. Based on the theory of elastoplastic bending of 2D beams, and supposing that the sheet is in plane deformation, the bending moments can be calculated.

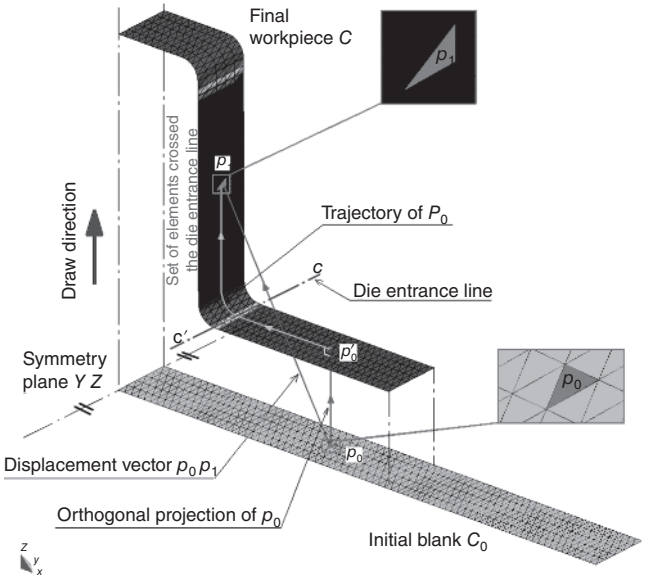

Figure 1.15 Deformation path prediction for an element.

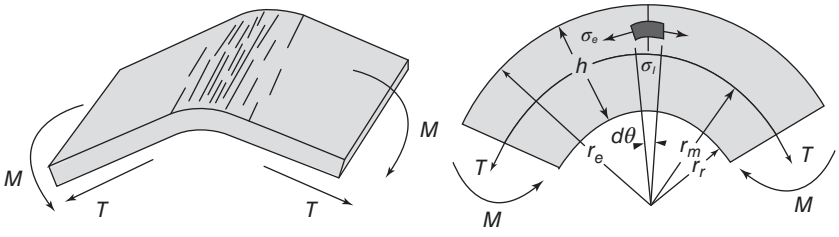

Figure 1.16 2D beam bending.

In the case of a planar beam in bending (Figure 1.16), if radial stresses are neglected, one can express the hoop stress as follows:

$$\begin{cases} \sigma_\theta = E\varepsilon_\theta & \rightarrow si \quad \bar{\varepsilon} \leq \varepsilon_y \\ \sigma_\theta = A\ K\ \bar{\varepsilon}^n & \rightarrow si \quad \bar{\varepsilon} > \varepsilon_y \end{cases} \tag{1.5}$$

with E the Young modulus, K and n the hardening coefficients, ε_y is the elastic limit of the material, $\bar{\varepsilon} = A\ \varepsilon_\theta$ the equivalent strain, and A is an anisotropy parameter.

For large strains, the logarithmic variation in z is generally used.

$$\varepsilon_\theta = \ln\left(1 + \frac{z}{r_m}\right) \tag{1.6}$$

Using a Lobatto integration scheme with *npl* points in the thickness (5 points in general), we can express the moment in the elastic zone M^e by

$$M^e = \sum_{i=1}^{npl} \omega_i \frac{z_e^2}{2} E(\zeta_i + 1) \ln\left(1 + \frac{z_e(\zeta_i + 1)}{2r_m}\right) \tag{1.7}$$

Similarly, the moment in the plastic zone M^p can be calculated with the following expression:

$$M^p = AK\sum_{i=1}^{npl}\omega_i \ \beta_i^n \left(\frac{z_e(1-\zeta_i)}{2} + \frac{h(1+\zeta_i)}{4}\right)\left(\frac{h-2z_e}{2}\right) \tag{1.8}$$

with $\beta_i = \ln\left(1 + \frac{0.5z_e(1-\zeta_i)+0.25h(1+\zeta_i)}{r_m}\right)$, npl the number of Lobatto points, ζ_i and ω_i represent the coordinates and weights of Lobatto points, respectively.

1.2.3.4 Bending and Unbending Problem

The following assumptions are retained in order to estimate the strains and the stresses in an element which initially was bent by crossing the die entrance line and then underwent unbending after leaving the die entrance radius.

- Bending occurs under the assumption of plane deformations.
- The cross-section before deformation remains constant after deformation.
- The bending of an element is obtained after three moments: ΔM^e an elastic bending due to a moment increment, ΔM^p a plastic bending due to a moment increment and finally an axial stretching ΔT.
- The Bauschinger effects are not taken into account; only isotropic work hardening governs re-plastification in the opposite direction of the loading.

Figure 1.17 shows an element undergoing elastoplastic bending and uniform stretching until it becomes straight. Consideration of uniform stretching, in addition to unbending of an element, is necessary to ensure that the sheet remains in tension after unbending.

It is assumed that elastic bending due to the increase in elastic moment ΔM^e occurs first until plasticity in the opposite direction of the bending. In the case of a kinematic hardening, the re-plastification begins when the bending moment reaches twice the value of the initial yield moment $2M_{\text{yl}}$, or else the stress reaches double the value of the yield stress $2\sigma_{\text{yl}}$. It is shown that after elastic bending due to the moment, the curvature of the sheet is reduced by a value of $\Delta\chi^e$. In the case of an isotropic work hardening, the re-plastification begins when the bending moment reaches twice the value of the moment at the end of loading $2M^{\text{total}}$, or else the stress reaches double the value of the stress at the end of loading $2\sigma^{\text{total}}$.

In order to unfold the sheet (the element), plastic deflection due to the bending moment ΔM^p and an elongation $\Delta\varepsilon_T$ will occur until the sheet becomes flat (the element becomes straight), because the curvature of the element becomes zero. It is assumed that the change in curvature during plastic bending $\Delta\chi^p$ is given by

$$\Delta\chi^p = \chi^{\text{total}} - \Delta\chi^e \tag{1.9}$$

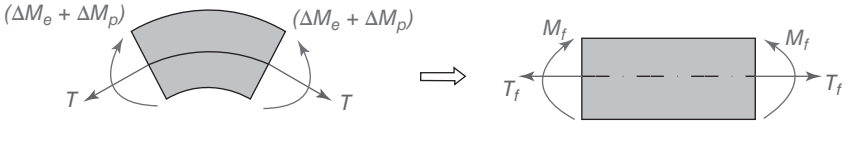

Figure 1.17 Elastoplastic bending/unbending of an element.

with χ^{total} the total curvature obtained at the end of loading or at the end of bending before the sheet (or the element) leaves the surface of the die.

1.2.3.5 Application to the Square Box of Numisheet93

The square box proposed in detail as a benchmark in the Numisheet93 conference involves the deep drawing of a box with constant radii of 8 mm and a depth of 25 mm, starting from a square blank of 150 mm × 150 mm (Figure 1.18). In all, 8628 shell elements were used for the forming simulation using the Improved Inverse Method and 4096 quadrilateral S4R shell elements for the simulation using ABAQUS standard (Figure 1.19).

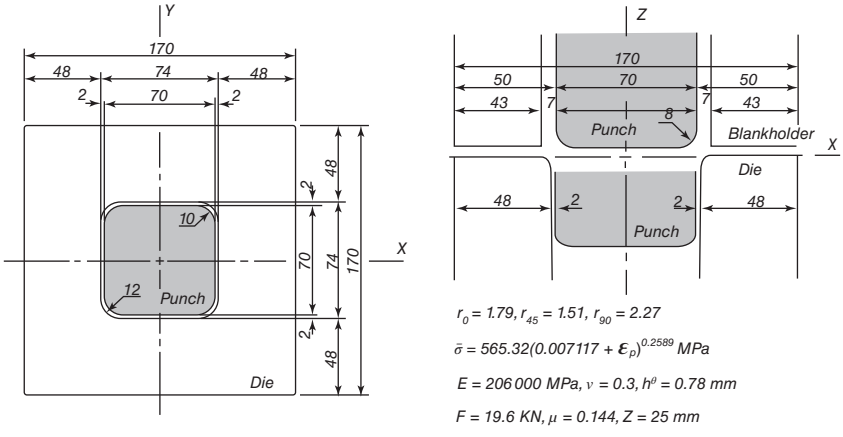

Figure 1.18 Geometrical and mechanical description of Numisheet93 square box.

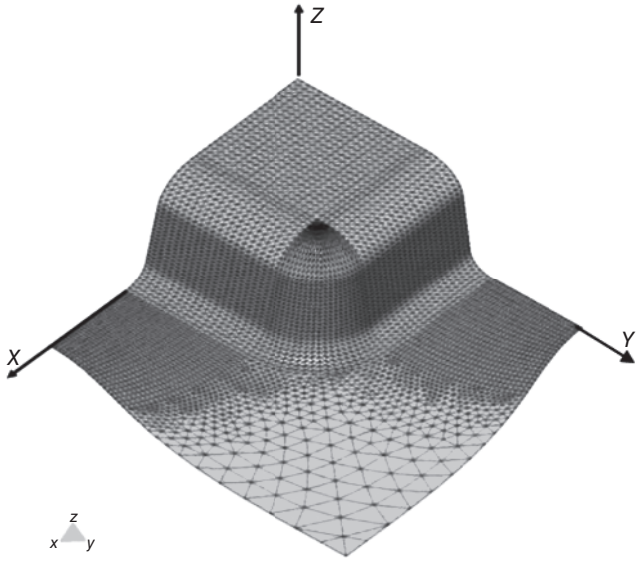

Figure 1.19 Quarter mesh of Numisheet93 square box.

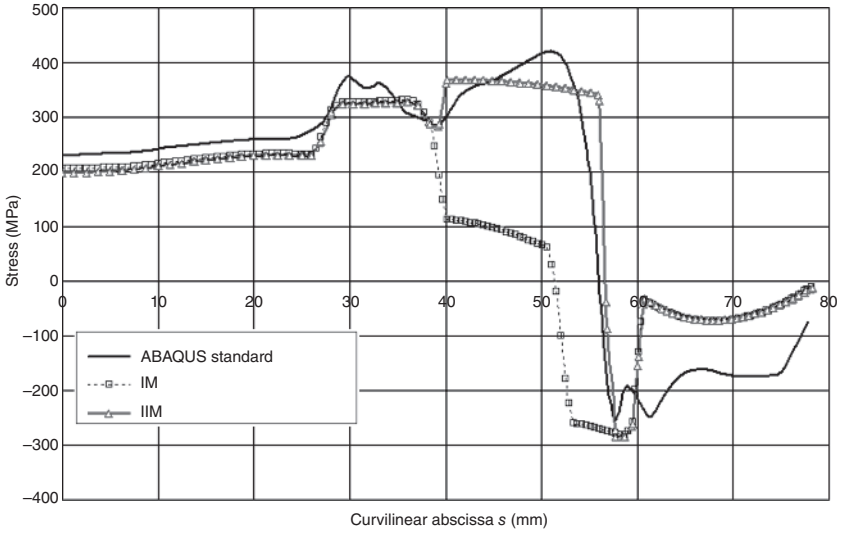

Figure 1.20 Distribution of the maximum stress on the upper layer.

To analyze the obtained results, the evolution of the maximum stress on the upper layer of the box along the *XZ* plane of symmetry is plotted as shown in Figure 1.20. One can remark that unlike the standard Inverse Method, the Improved Inverse Method allows a good prediction of stresses especially in the potential zone between the die entrance line and the punch, i.e. 40 mm $\leq s \leq$ 60 mm.

Figure 1.21 shows the distribution of the maximum stress on the upper layer of the square box obtained by the Inverse Method before and after improvement as well as the reference solution of ABAQUS standard. One can notice that the Improved Inverse Method allows the detection of the potential area of elements which have undergone bending and unbending effects and improve the stresses in the part of the free strand (free area between the punch and the die radius). Hence, the Improved Inverse Method becomes of a great interest in simulating the springback effects at the end of the stamping.

1.3 Optimization of Stamping and Hydroforming Parameters

Perhaps one of the most important added values of the numerical simulation of sheet metal forming processes such as stamping and hydroforming is to help the user understand the material deformation process involved during the forming of the workpiece for given operating conditions. The main objective is to produce parts which meet the customer's specifications. Understanding the material deformation process allows a user with a significant metal forming knowledge to control and modify the process conditions avoiding fracture and wrinkling risks.

As soon as the finite element simulation codes based either on explicit dynamics or implicit statics were shown to predict accurately the quality of the final

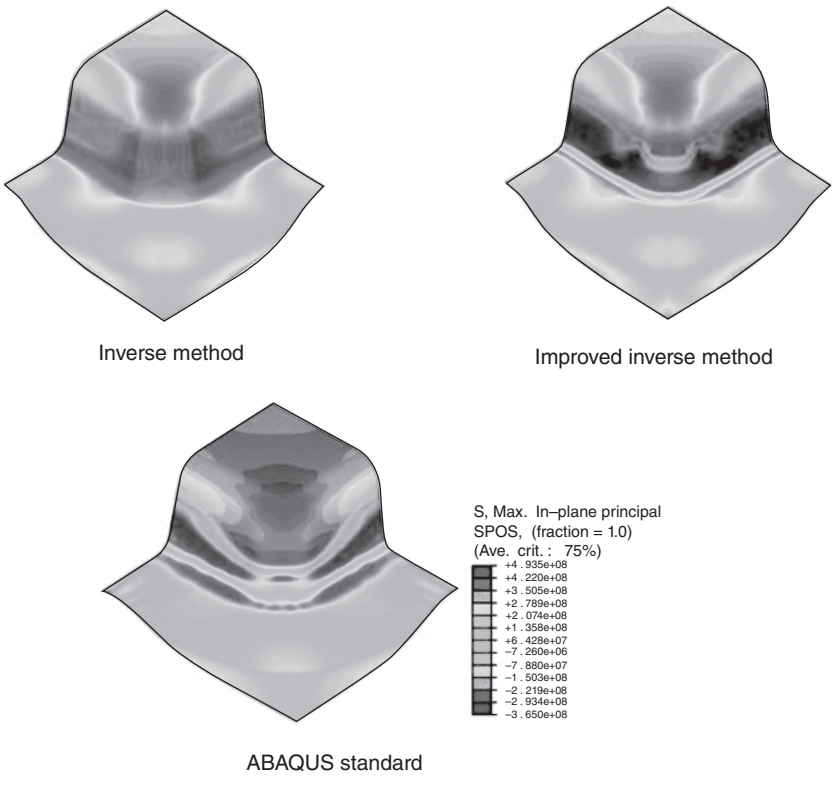

Figure 1.21 Distribution of the maximum stress on the upper layer.

workpiece, different research groups proposed to introduce the mathematical optimization problem to automatically predict "ideal" values of some key forming process parameters in order to obtain a defect-free workpiece. The goal here was the prediction of the best sheet metal forming conditions for a given CAD geometry.

This section does not intend to be exhaustive and cover all recent research works on the optimization of stamping and hydroforming processes parameters, since the number of research investigations on this topic is extensive. In this section, a brief overview of recent research related to the optimization of sheet metal forming is presented.

One can group the investigations from the simplest to the most difficult from the numerical implementation point of view:

- the geometry and position of the initial blank,
- the holding pressure exerted by the blankholder, the position and geometry of the drawbeads,
- the tool geometry (to control the springback),
- the nature and quantity of the lubricant,
- the blank material,
- the nature of tools.

1.3.1 Mathematical Optimization Problem

Most of the applications presented in this chapter were solved using mathematical programming methods where the objective was the numerical resolution of the optimization problem. The optimization problem can be stated as follows:

$$\begin{aligned} & Min\ f(v_i) \\ \text{with} \quad & g_j(v_i) \le 0 \qquad j = 1, m \\ & h_l(v_i) = 0 \qquad l = 1, m_e \\ & v_{i\min} \le v_i \le v_{i\max} \qquad i = 1, n \end{aligned} \tag{1.10}$$

where f is the objective or cost function to be minimized according to the design variables v_i, and g_j and h_l are the inequality and equality constraints respectively.

Design variables are the sheet metal forming process parameters chosen to be modified. The objective and constraint functions aim to describe in mathematical form the objective of producing a defect-free workpiece. The constraints functions also make it possible to introduce geometrical bounds on the design variables. From the mathematical point of view, the chosen functions must reproduce the user desire in producing a final workpiece by avoiding fracture and wrinkling [30, 31, 34]. Therefore, it becomes necessary to be able to translate into a mathematical form the concept of a "defect-free" part from the mechanical state estimated using numerical simulation. The determination of "good" objective and constraint functions will not be detailed in this section. Interested readers are invited to refer to the references.

1.3.2 Shape Optimization of the Initial Blank

In early 1996, we proposed to optimize the shape of the initial blank [35]. The design variables are the control knots distributed on the contour of the initial blank and used to build a cubic B-spline parametrization. Different objective functions were tested. They used variations in thickness to control the risks of excessive thinning, which precedes the metallic sheet fracture and the risks of thickening, which reflects a tendency for wrinkling. Numerical simulations were performed using an Inverse Method to solve the stamping problem in a single step, coupled with an optimization algorithm based on Sequential Quadratic Programming method. The gradients of the objective function and constraints were calculated using the adjoint state variable method, i.e. analytically in our in-house stamping software FASTSTAMP© [31]. The procedure was applied to the optimization of a Twingo car dashpot cup (Figure 1.22). The initial blank contour was described using eight control knots. Therefore, 16 design variables were generated. Convergence was achieved after 20 iterations. The thinning evolved from an initial value of −20.27% to −12.92% and the thickening evolved from 17.44% to a final optimal value of 13.41%.

During the first presentations of these results, criticisms were raised on the complexity shape of the contour which is difficult to cut in an industrial context of high production rate. It seems that the introduction of a laser cutting portal and the increase in the price of steel make nowadays this type of optimization more interesting.

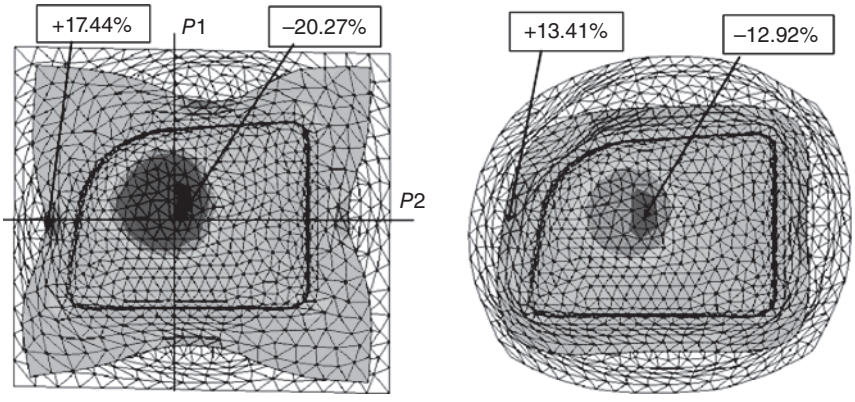

Figure 1.22 Optimization of a Twingo car dashpot cup: initial and optimal contour.

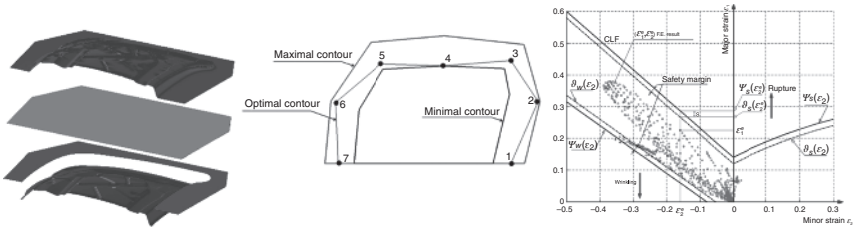

Figure 1.23 Blank shape optimization procedure in the stamping process.

However, an alternative method has been proposed for working on blank contours by using line segments. The design variables are the coordinates of segments intersections. The optimization problem is solved by carrying out an approximation of the objective function and constraints using diffuse approximation (or weighted least squares method). An optimization algorithm solves the approximated problem. It is possible to improve the solution obtained by carrying out a second design of experiments located around the first identified optimum. This technique has been successfully applied in the optimization of several industrial applications (Figure 1.23).

1.3.3 Optimization of Addendum Surfaces of Stamped Parts

A variant of topology family method called "Evolutionary Structural Optimization" or ESO for the topological optimization of structures and mechanical parts has been proposed by Xie and Steven. This method is based on the concept of progressive removal of ineffective material from the structure. Thus, the structure will evolve from a large very simple shape (usually rectangular) to the desired optimal shape (usually complex).

Compared to other structural optimization techniques, such as the homogenization method and the density function method, the ESO method is very attractive because of its simplicity and efficiency. Recently, it has been demonstrated that the ESO method can solve a variety of problems of shape and topology optimization, in statics, dynamics, and buckling.

The ESO technique has been implemented and evaluated for the shape optimization of addendum surfaces for the stamping of three-dimensional workpieces by exploiting the main advantages of the inverse method which are speed and functionality.

After evaluating the ESO technique, one can conclude that the shape optimization of addendum surfaces in sheet metal stamping can be solved in a simple and effective way using the evolutionary optimization procedure. Indeed, the obtained shape of the blank contour at each ESO state can be chosen as an effective design. Thus, the ESO method can offer to designers several optimal configurations during the preliminary design stage of a prototype. For our applications, only constraints on the volume of material have been imposed, and the evolutionary design which satisfies the constraints is considered to be optimal.

From a theoretical point of view, there are a few points to study. In particular, the reduction in the total number of iterations of the optimization process, especially when approaching the optimum where 40% of iterations are done without a substantial improve of the objective function.

Another point of reflection concerns the optimization criteria, since a good choice of the criterion is decisive in obtaining a good final optimal solution. This point remains crucial because it can only be done in concert with manufacturers.

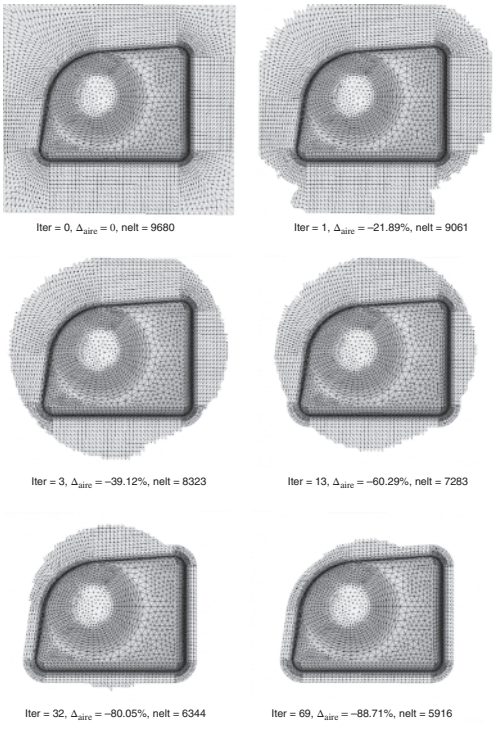

Figure 1.24 Topology optimization of addendum surfaces: (a) addendum surface of Twingo dashpot, (b) convergence process. Source: (b) Hakim Naceur.

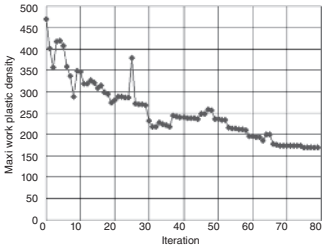

(b)

Figure 1.24 (*Continued*)

This method has been successfully applied for the determination of optimal addendum surfaces for industrial parts (Figure 1.24). The technical details relating to this method can be found in the references [25, 26].

1.3.4 Optimization of Drawbead Restraining Forces

A drawbead is a baffle located in the die under the blankholder zone on the trajectory of the metallic sheet flow and whose role is to slow down the sliding of the metallic sheet according to its geometry (Figure 1.25). The geometry of the drawbead is

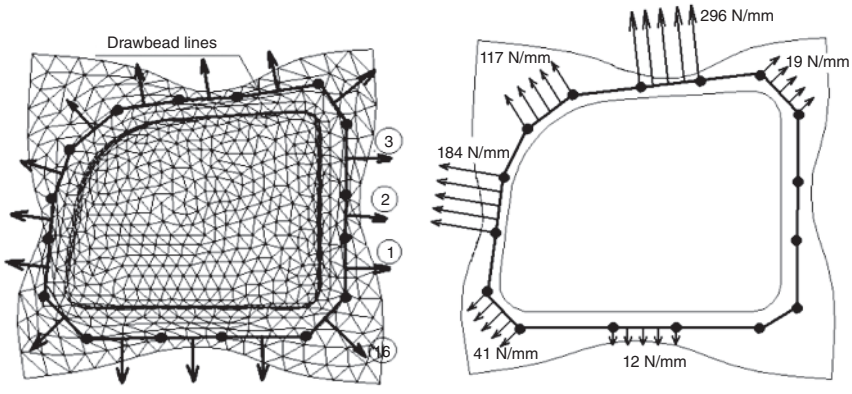

(a)

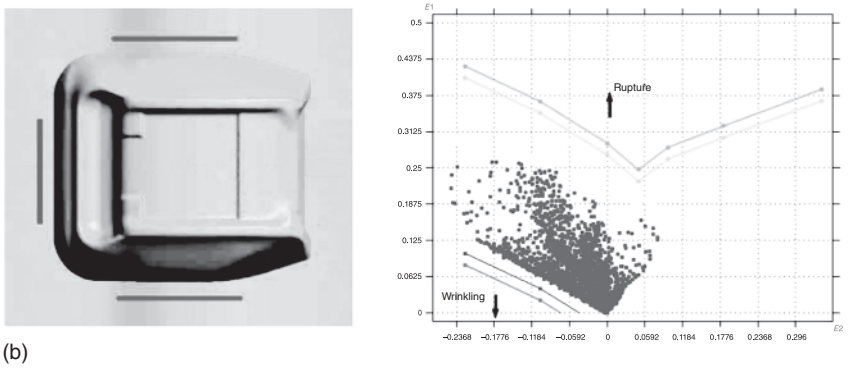

(b)

Figure 1.25 Optimization of drawbead restraining forces in the stamping of industrial parts (dashpot cup and oil pan).

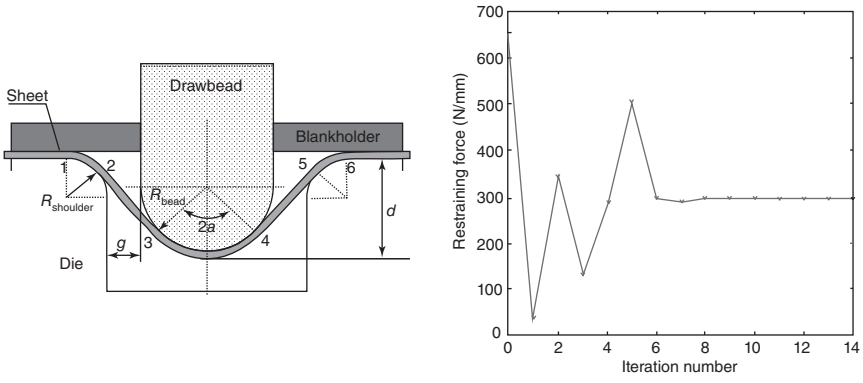

Figure 1.26 Geometrical description of a drawbead used in stamping.

not of the same order of magnitude as the dimensions of the piece to be formed. A numerical simulation which integrates the contact-friction between the sheet and the drawbead will be costly in terms of CPU computing time. In particular, it will be necessary to locally use a fine mesh in the area of the drawbead, while the part under blankholder is generally not in the useful part of the workpiece and disappears in the post-stamping operations (e.g. cutting).

In professional stamping software, the modeling of the drawbeads is carried out by the introduction of retaining forces. These forces are either calculated using analytical models or using finite element simulation in 2D with the assumption plane strains.

An approach is proposed here to optimize the drawbead restraining forces. Figure 1.26 shows an example of design of drawbead restraining forces. Sixteen drawbead lines were used for the benchmark of the Twingo dashpot cup. The Inverse Method was used to simulate the stamping process. The aim of optimization was to minimize thickness variations in order to minimize risks of rupture and wrinkling.

Convergence was obtained after 35 iterations. The thinning evolved from −18.04% to −17.39% and the thickening from 25.74% to 22.26%. Numerically the values of the drawbead restraining forces are optimized and then need to build up the corresponding drawbead geometries. An optimization procedure has been developed for this task; it is based on an analytical response of a 2D drawbead restraining force to perform its design [32–34]. This involves determining the geometry of the drawbead which allows obtaining the optimal drawbead restraining force to be produced to generate a defect-free workpiece.

Knowing the drawbead geometry and the physical properties of the metallic sheet, one can estimate the drawbead restraining force using the analytical model of Stoughton. At this stage, it is a question of solving an inverse problem: identify the geometry of the drawbead which is capable of producing the imposed optimal drawbead restraining force found previously. Now the design variables are the geometric characteristics of the drawbead, namely, the radius R_{shoulder}, the radius R_{drawbead}, etc. Our goal is to obtain at the end of the optimization process a retaining force equal to the imposed optimal one. Moreover, the drawbead restraining force has to be

distributed as uniformly as possible along the drawbead line. The objective function in this case was chosen as the mean difference between the bending/unbending forces. This 2D simulation is very fast since it is based on the analytical drawbead model. It must be carried out for each of the forces found in the first stage, i.e. the design procedure will be repeated for each drawbead line.

1.3.5 Optimization of Tool Geometry

The prediction of springback is directly influenced by numerical parameters involved in the forming process, such as element size and type, punch velocity, pressure control, contact treatment, tools discretization, etc. But also it depends on physical parameters of the forming process, such as material hardening, geometry of workpiece, holding forces, temperature, etc.

From the numerical simulation point of view, the most important point is to obtain a precise stress state at the end of the sheet metal forming process. The springback simulation can be carried out numerically in different ways.

- A full simulation with tool contact treatment.
- A simplified simulation using external forces to replace the tool actions.
- A simplified simulation considering only the residual stresses at the end of the forming process.

As part of our research investigation in this topic, a co-simulation has been carried out by coupling of two codes: one FE software for the forming simulation and the other FE software for structural analysis. Special numerical procedures for field exchange interface were developed for communication between the two codes. A numerical procedure was also developed for tool (punch and die) radii optimization based on the minimization of residual stresses in the workpiece after tool removal (Figure 1.27). The objective was to determine optimal tool radii which minimize the opening distance d_i as shown in Figure 1.28 [29].

Punch radius R_p and matrix radius R_d were considered as design variables, while the objective function represented the opening distance d_i (Figure 1.28).

$$J = \sum_{i=1}^{nnt} \{d_i\}^T \{d_i\} = \sum_{i=1}^{nnt} (u_{X_i}^2 + u_{Y_i}^2 + u_{Z_i}^2) \tag{1.11}$$

The optimization problem was solved with an optimization procedure based on moving least square response surface method. An initial grid of 6×6 equidistant knots was used to evaluate the objective function with the following constraints:

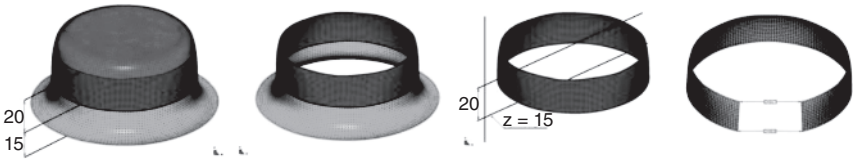

Figure 1.27 Demeri spring back benchmark.

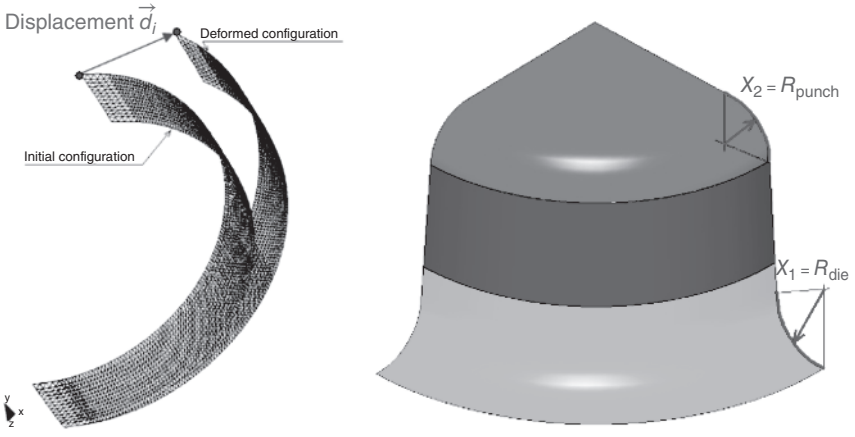

Figure 1.28 Spring back optimization problem based on tools design.

$R_{min} = 2$ mm and $R_{max} = 23$ mm. Convergence was achieved in 15 iterations leading to an optimal solution corresponding to a punch radius of $R_p = 4.13$ mm and a die radius of $R_d = 21.4$ mm.

1.3.6 Optimization of Material Parameters

Regarding the material properties, the aim of the research investigation was to identify optimal material characteristics which allow the successful forming of a given CAD geometry.

Forming limit curves were used to detect the risks of fracture and wrinkling in the final workpiece. The forming process simulation was carried out using an Inverse Method. The wrinkling was estimated according to the compressive stress state on each finite element located on the addendum surfaces. As shown in Figure 1.29, the forming limit diagram depends on the material and the deformation path. For each new material used during optimization a curve is determined using the model of Marciniak and Kuczynski.

Here the design variables are the hardening exponent n of the Swift–Voce law $\overline{\sigma}_{Swift} = A(\varepsilon_0 + \overline{\varepsilon}_p)^n$ and the Lankford anisotropy coefficient r.

The method was applied to solve several benchmarks. In particular, for the square box benchmark of Numisheet93, two materials, a steel and an aluminum alloy, were proposed to carry out experimental tests and numerical simulations. It was found that the proposed aluminum did not allow to exceed a forming depth more than 20 mm without fracture. A stamped box of 23 mm depth was then chosen. For this case, two optimization methods were used. The first was based on a metamodeling approach by using a diffuse response surface approximation coupled to Box–Behnken design of experiment and the second used a Sequential Quadratic Programming algorithm.

Table 1.2 summarizes the principal results obtained using both optimization procedures. The initial values were the properties of the aluminum alloy which has

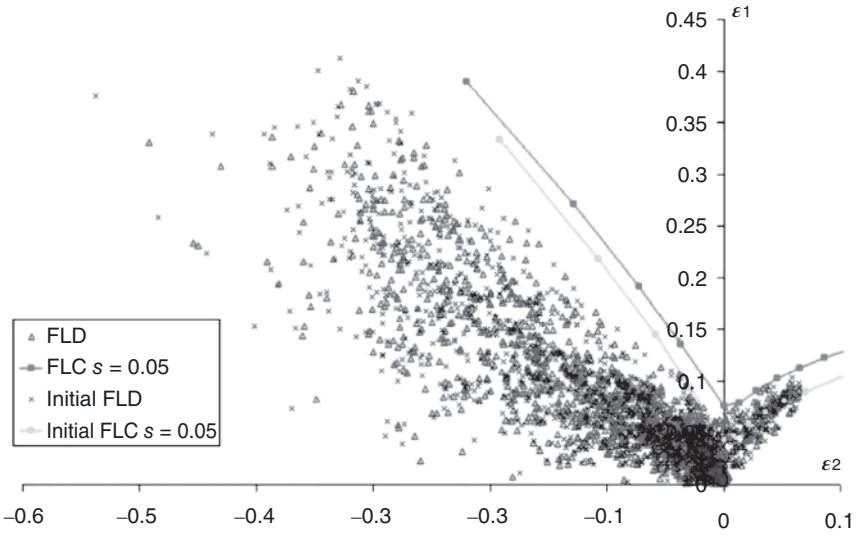

Figure 1.29 Forming limit diagram before and after optimization.

Table 1.2 Optimization of material parameters.

Material	n	r	R_w	Δt_{min} (%)	Δt_{max} (%)	Objective function evaluations	Iterates
Aluminum	0.36	0.64	10.4	−35.6	16.2		
Steel	0.26	1.77	5.85	−10.1	9.5		
Metamodel	0.19	1.93	3.81	−9.7	11.1	26	7
SQP	0.24	1.95	5	−9.9	10.8	48	12

knots above the forming limit curve (not shown). The wrinkling factor was $R_w = 10.4$. The objective was to avoid knots going above the forming limit curve using a wrinkling factor $R_w = 5$. This is achieved by the two optimization procedures. The properties obtained at the end of the optimization procedures tend toward the values of steel, which was proposed at Numisheet93. We also noticed a decrease in the minimum and maximum values of the thickness variation $\Delta t_{\min}$ and $\Delta t_{\max}$.

The two optimization procedures are deterministic and the obtained results are different for the hardening exponent n but gave slightly the same Lankford anisotropy coefficient r as shown in Table 1.2. In terms of thickness variation, both optimization procedures gave approximately the same results with −10% of thinning and +11% of thickening (Figure 1.30).

The main assumptions of this work were to consider that material properties are continuous, and assume that any values of the couple (n, r) exists. This is not completely false since the anisotropy comes essentially from the rolling operation. If we optimize the preliminary rolling stage of the metallic sheet and also optimize the

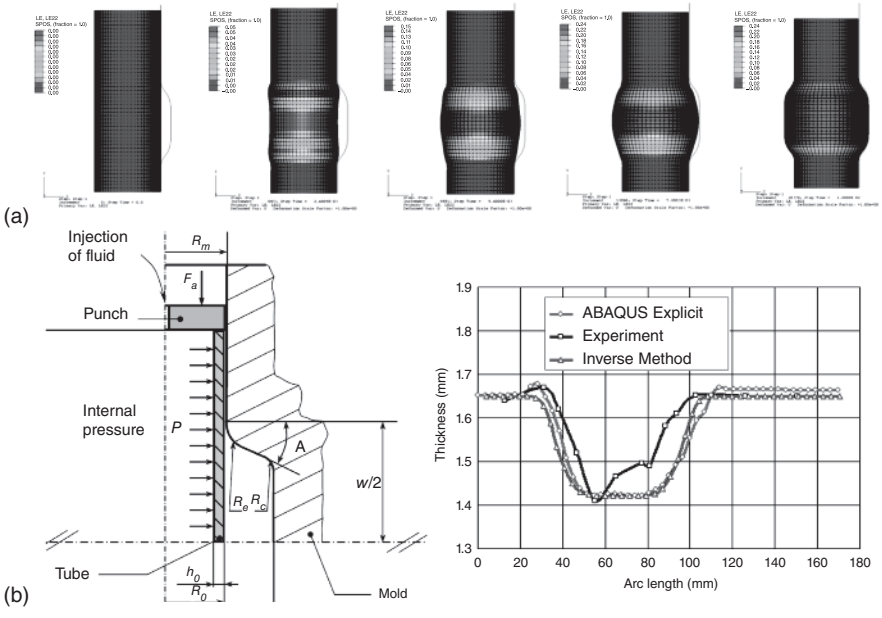

Figure 1.30 Tube hydroforming results comparison: simulation versus experiment.

heat treatments conditions, it is possible to obtain the desired material, but the price of this procedure may be prohibitive.

1.3.7 Optimization of Hydroforming Process Parameters

This section deals with the formulation, development, and simulation of a three-dimensional hydroforming process based on an inverse method for the rapid analysis in order to optimize the parameters of this forming process.

Knowing some limitations to generate tube CAD geometry, tube thickness distribution has to be as uniform as possible at the end of hydroforming process. During the hydroforming process, compressed and expanded zones may appear simultaneously in the workpiece. As a result, the calibration of process becomes a challenge since tedious optimization of successive hydroforming stages are mandatory. Although experimentation on surrogate models seems necessary, it will nevertheless be difficult to extrapolate calibration tasks to a real industrial part, especially for hydroforming of tubes which makes the situation more complex, since in the forming process usually some preliminary stages of bending and calibration are necessary.

The optimization concerns the process operating parameters such as the friction conditions, the pressure and backpressure control, the drawbead forces, the rheology of material or initial thicknesses, and the tool geometry to take account for springback estimation. The results obtained with different types of material data, geometries, and operating conditions are compared with the objectives or targets defined in conjunction with industrial needs (see references [27, 28]).

The use of a rapid simulation method makes it possible to consider a large number of evaluations of quality functions.

A typical example consists in determining the optimal length L_0 of the initial tube as well as the "ideal" properties of the material, which can be described simply by the coefficients of the Swift–Voce hardening law (K, n) so as to obtain a final "feasible" tube (without necking nor wrinkling) as well as a minimal plastic work. The objective function chosen for this purpose can be expressed as

$$f = \sum_{e=1}^{\text{nelt}} f^e; \quad \text{with} \quad f^e = \int_V \left(\int_0^{\bar{\varepsilon}_p} \bar{\sigma} d\bar{\varepsilon}_p \right) dV \tag{1.12}$$

where $\bar{\varepsilon}_p$ is the total equivalent plastic strain, V is the total volume of the workpiece and $\bar{\sigma}$ is the equivalent stress depending on the hardening type, for instance if the combined Swift–Voce law is used, then the equivalent stress is

$$\begin{aligned} & \bar{\sigma} = \alpha \ \bar{\sigma}_{\text{Swift}} + (1-\alpha) \ \bar{\sigma}_{\text{Voce}} \\ \text{with} \quad & \bar{\sigma}_{\text{Swift}} = A(\varepsilon_0 + \bar{\varepsilon}_p)^n \\ & \bar{\sigma}_{\text{Voce}} = k_0 + Q(1 - \exp(-\beta \bar{\varepsilon}_p) \end{aligned} \tag{1.13}$$

In practice, nonlinear constraints are imposed on the design variables, so as to avoid obtaining non-feasible solutions. For this purpose, the thickness variation of the tube will generally be limited between −20% as a lower value and +15% as a higher limit. It is also important to impose geometric constraints on the design variables (tube length L_0 and material hardening exponent n). The optimization problem can be stated as

$$\begin{aligned} \textit{Min} \quad & f(L_0, n) = \sum_{e=1}^{nelt} \int_V \left(\int_0^{\bar{\varepsilon}_p} \bar{\sigma} d\bar{\varepsilon}_p \right) dV \\ \text{with} \quad & \lambda_z^{\max} \leq 1.15 \\ & \lambda_z^{\min} \geq 0.8 \\ & 150 \ \text{mm} \leq L_0 \leq 200 \ \text{mm} \\ & 0.1 \leq n \leq 0.6 \end{aligned} \tag{1.14}$$

where $\lambda_z = t/t_0$ is the stretch, t and t_0 are the thickness and initial thickness respectively. At the beginning, a design of experiment based on the central composite algorithm was used for the construction of response surface in order to estimate the cost function. Then a normalization of the variables (between −1 and +1) is used in order to guarantee a stability of the optimization algorithm and to facilitate the data processing. A global response surface based on the diffuse approximation was built using the design of experiment already prepared, and the final result is shown in Figure 1.31.

The minimization of the objective function, under constraints, was done by using a Sequential Quadratic Programming algorithm based on the work of Powell M.J.D. using multiple starting initial solutions. The optimal solution was obtained in only four iterations, allowing an optimal solution corresponding to $L_0 = 178.82$ mm, $n = 0.59$.

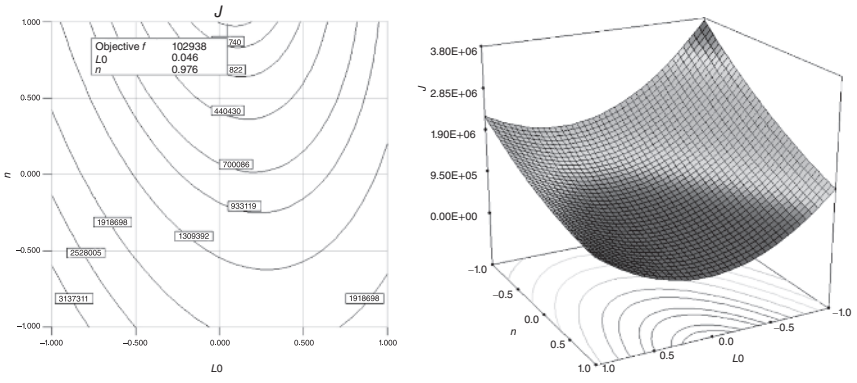

Figure 1.31 Global diffuse response surface approximation for the optimization of tube hydroforming process parameters.

1.4 Future Outlooks

Nowadays, the most economical technique for obtaining a car body part is still stamping. However, each stamped part has defects, which can be classified as: "aspects defects" and "geometrical defects." For the calculation of geometrical defects, quality requirements mean that one can no longer reason on a single stamped part but rather on a group of parts because after assembly, the stamped workpiece will be part of a complex assembly (e.g. car body in white) forming the overall vehicle body.

In order to fulfill the requirements of obtaining a "good quality" vehicle body, it is crucial to analyze the interactions between all the involved parts. Thus, the final result of the assembly deformation (Figure 1.32) is dependent on many local parameters such as part stiffnesses, sheet metal thicknesses, material parameters, and so on or global parameters such as positions and number of weld joints, modeling of boundary conditions, types of finite element models, and so on.

The scope of future developments is as follows:

- The development of numerical procedures to take into account uncertainty of the forming process parameters (local and global) on the overall quality of the final assembly (springback, residual stresses in the full assembly). This will allow the definition of tolerance margins on elementary parts when they are initially processed using stamping or hydroforming followed by springback operations, during the early design or pre-project phases.
- A second step would be to carry out optimization procedures based on meta models and artificial intelligence for the robust optimization of assembly defects (due to springback, residual stresses, etc.) by using local and/or global forming process parameters and their variability.

1.5 Conclusions

Deep drawing and hydroforming processes are very important for several industrial sectors and the simulation of these processes needs to be continuously enhanced. In the future, several investigations may be followed to achieve this target. The numerical applications presented previously, have shown the importance of mastering the process parameters in order to control the mechanical behavior of the final workpiece obtained using either stamping or hydroforming. Nowadays, the use of various numerical optimization algorithms coupled to explicit/implicit nonlinear forming solvers has gained maturity and has allowed a quasi-automatic design of numerous process parameters to achieve a final workpiece without defects such as wrinkling or fracture. However, in the last few years, new challenging expectations have arisen regarding a higher level of quality commitment of sheet metal forming parts obtained by deep drawing and hydroforming. In particular, for the automotive and the aeronautical industries, it is becoming important to ensure at the end of forming simulations (stamping or hydroforming) that the final "defect-free" workpiece satisfy specific requirements regarding a higher level of crash safety while maintaining a reduction of overall weight. The new level of parameter design will be the coupling of optimization algorithms with a set of nonlinear solvers successively (such as buckling, crash/impact, durability, and so on) to assess the workpiece quality. Therefore, it will be possible, at the early design stage, to design some key process parameters using specific objective functions and constraints to improve the part in service life expectancy. Therefore, the final workpiece will be not only a "defect-free" part but also a part with an "optimal" strength to weight ratio.

Mathematical optimization is currently used to calculate the best process parameters. Expert systems allow an initial adjustment which may or not be refined by optimization to avoid process instability problems. It is therefore a matter of robustness. A change in the process parameters should not have much influence on the quality of parts obtained using deep drawing or hydroforming.

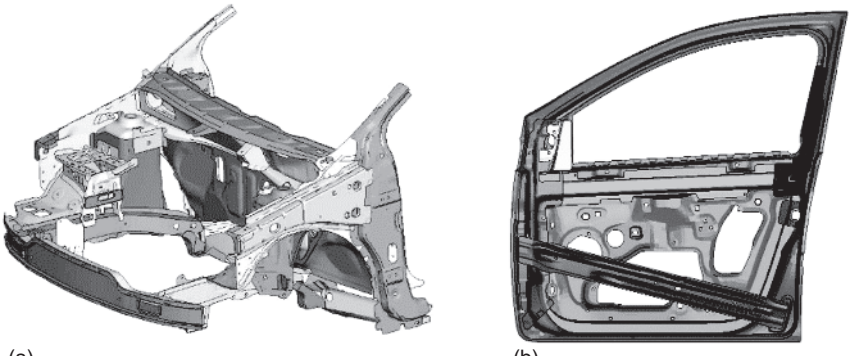

Figure 1.32 Uncertainty simulation in assemblies of stamped parts constituting an automobile body in white. Source: (b) Hakim Naceur.

References

1 Kang, B.S., Son, B.M., and Kim, J. (2004). A comparative study of stamping and hydroforming processes for an automobile fuel tank using FEM. *International Journal of Machine Tools and Manufacture* 44 (1): 87–94.

2 Lang, L.H., Wang, Z.R., Kang, D.C. et al. (2004). Hydroforming highlights: sheet hydroforming and tube hydroforming. *Journal of Materials Processing Technology* 151 (1–3): 165–177.

3 Singh, S.K. and Kumar, D.R. (2008). Effect of process parameters on product surface finish and thickness variation in hydro-mechanical deep drawing. *Journal of Materials Processing Technology* 204 (1–3): 169–178.

4 Geiger, M., Merklein, M., and Cojutti, M. (2009). Hydroforming of inhomogeneous sheet pairs with counter pressure. *Production Engineering* 3 (1): 17–22.

5 Modi, B. and Kumar, D.R. (2019). Optimization of process parameters to enhance formability of AA 5182 alloy in deep drawing of square cups by hydroforming. *Journal of Mechanical Science and Technology* 33 (11): 5337–5346.

6 Bell, C., Corney, J., and Savings, D. (2020). A state of the art review of hydroforming technology. *International Journal of Material Forming* 13: 789–828.

7 Nguyen, B.N., Johnson, K.I., and Khaleel, M.A. (2003). Analysis of tube hydroforming by means of an inverse approach. *Journal of Manufacturing Science and Engineering* 125 (2): 369–377.

8 Guo, Y.Q., Batoz, J.L., Detraux, J.M., and Duroux, P. (1990). Finite element procedures for strain estimations of sheet metal forming parts. *International Journal for Numerical Methods in Engineering* 30 (8): 1385–1401.

9 Guo, Y.Q., Batoz, J.L., Naceur, H. et al. (2000). Recent developments on the analysis and optimum design of sheet metal forming parts using a simplified inverse approach. *Computers & Structures* 78 (1–3): 133–148.

10 Batoz, J.L., Guo, Y.Q., and Mercier, F. (1998). The inverse approach with simple triangular shell elements for large strain predictions of sheet metal forming parts. *Engineering Computations* 15 (7): 864–892.

11 Chung, K., Barlat, F., Brem, J.C. et al. (1997). Blank shape design for a planar anisotropic sheet based on ideal forming design theory and FEM analysis. *International Journal of Mechanical Sciences* 39 (1): 105–120.

12 Chung, K., Yoon, J.W., and Richmond, O. (2000). Ideal sheet forming with frictional constraints. *International Journal of Plasticity* 16 (6): 595–610.

13 Lee, C.H. and Huh, H. (1998). Blank design and strain estimates for sheet metal forming processes by a finite element inverse approach with initial guess of linear deformation. *Journal of Materials Processing Technology* 82 (1–3): 145–155.

14 Naceur, H. (1999). Etude comparative de deux méthodes pour la simulation inverse de l'emboutissage des tôles minces. In: *Rapport interne de recherche*, 120. Edition: Université de Technologie de Compiègne, 53 pages, Compiègne.

15 Guo, Y.Q., Naceur, H., Debray, K., and Bogard, F. (2003). Initial solution estimation to speed up inverse approach in stamping modeling. *International Journal for Computer-Aided Engineering* 20 (7): 810–834.

16 Naceur, H., Guo, Y.Q., and Gati, W. (2002). New enhancements in the inverse approach for the fast modeling of autobody stamping process. *International Journal of Computational Engineering Science* 3 (4): 355–384.

17 Naceur, H., Ben, E.S., Batoz, J.L., and Knopf-Lenoir, C. (2008). Response surface methodology for the rapid design of aluminium sheet metal forming parameters. *Materials & Design* 29 (4): 781–790.

18 Naceur, H., Delamzire, A., Batoz, J.L. et al. (2004). Some improvements on the optimum process design in deep drawing using the inverse approach. *Journal of Material Processing Technology* 146 (2): 250–262.

19 Batoz, J.L., Naceur, H., and Guo, Y.Q. (2007). Sheet metal stamping analysis and process design based on the inverse approach. In: *10th Esaform Conference on Material Forming*, Zaragoza, Spain (18–20 April). American Institute of Physics.

20 Gati, W., Guo, Y.Q., Naceur, H., and Batoz, J.L. (2003). Approche Pseudo Inverse pour estimation des contraintes dans les pices embouties axisymtriques. *European Journal of Computational Mechanics* 12 (7–8): 863–886.

21 Gati, W., Guo, Y.Q., Naceur, H., and Batoz, J.L. (2002). An efficient pseudo inverse approach for stress evaluation in sheet forming modelling. In: *NUMISHEET2002*, Jeju Island, Korea (21–26 October), vol. 1, 295–300.

22 Guo, Y.Q., Gati, W., Naceur, H., and Batoz, J.L. (2001). Stress evaluation in sheet forming modeling by inverse approach for springback simulation. In: *7th European Conference on Advanced Materials and Processes*, Rimini, Italy (10–14 June).

23 Breitkopf, P., Naceur, H., Rassineux, A., and Villon, P. (2005). Moving least squares response surface approximation: formulation and metal forming applications. *Computers & Structures* 83 (17–18): 1411–1428.

24 Ben, E.S., Naceur, H., and Batoz, J.L. (2005). Simulation de l'emboutissage par approche inverse amliore pour l'estimation du retour lastique. *European Journal of Computational Mechanics* 14 (8): 957–984.

25 Ben, E.S. and Naceur, H. (2006). Optimisation topologique de surfaces additionnelles de tles embouties. *European Journal of Computational Mechanics* 15 (7–8): 909–943.

26 Naceur, H., Guo, Y.Q., and Batoz, J.L. (2004). Blank optimization in sheet metal forming using an evolutionary algorithm. *Journal of Materials Processing Technology* 151: 183–191.

27 Chebbah, M.S., Naceur, H., Hecini, M., and Belouettar, S. (2007). Response surface method for the rapid design of process parameters in tube hydroforming. In: *9th International Conference on Numerical Methods in Industrial Forming Processes*, Porto, Portugal (17–21 June), vol. 908, 455–460.

28 Chebbah, M.S., Naceur, H., and Belouettar, S. (2007). Material parameters and blank optimization for springback compensation in sheet metal forming. In: *1er Congrs Algrien de Mcanique de Construction*, Algiers, Algeria (29–30 April).

29 Naceur, H., Guo, Y.Q., and Ben, E.S. (2006). Response surface methodology for the design of sheet forming parameters to control springback effects. *Computers & Structures* 84 (2627): 1651–1663.

30 Breitkopf, P., Naceur, H., Rassineux, A., and Villon, P. (2005). Optimizing metal forming process using response surface approximation and inverse approach. *International Journal of Forming Processes* 8: 13–29.

31 Batoz, J.L., Naceur, H., Delamzire, A. et al. (2002). Design of process parameters in deep drawing of sheets to improve manufacturing feasibility. In: *Integrated Design & Manufacturing in Mechanical Engineering*, 295–302. Kluwer Academic Publishers.

32 Naceur, H., Guo, Y.Q., Batoz, J.L., and Knopf-Lenoir, C. (2001). Optimization of drawbead restraining forces and drawbead design in sheet metal forming process. *International Journal of Mechanical Sciences* 43 (10): 2407–2434.

33 Naceur, H., Guo, Y.Q., Batoz, J.L., and Knopf-Lenoir, C. (2000). Optimisation des forces de retenue pour le contrle de la qualit des tles minces embouties. *European Journal of Computational Mechanics* 9 (1–3): 151–172.

34 Naceur, H. and Delamzire, A. (2007). Modlisation et optimisation de paramtres de procd en emboutissage de tles minces. In: *Modlisation numrique: dfis et perspectives*, vol. 1, 255–293. Edition Herms, Lavoisier. ISBN: 978-2-7462-1615-0.

35 Batoz, J.L., Naceur, H., Barlet, O. et al. (1996). Optimum design of blank contours in axisymmetrical deep drawing process. In: *Advances in Computational Mechanics* (eds. W. Zhong, G. Cheng and X. Li), 113–125. International Academic Publishers.